

Characteristics of solar diurnal variations: a case study based on records from the ground magnetic station at Vassouras, Brazil

Klausner V.^{a,b}, Papa A. R. R.^{a,c}, Mendes O. Jr.^b, Domingues M. O.^d, Frick P.^e

^aNational Observatory - ON 20921-400, RJ, Brazil

^bINPE/CEA/DGE National Institute for Space Research - INPE 12227-010 São José dos Campos, SP, Brazil

^cRio de Janeiro State University - UERJ, RJ, Brazil

^dINPE/CTE/LAC National Institute for Space Research - INPE 12227-010 São José dos Campos, SP, Brazil

^eInstitute of Continuous Media Mechanics, Perm, Russia

Abstract

The horizontal component amplitudes of magnetograms recorded by ground-based observatories of the INTERMAGNET network have been used to analyze the global pattern variance of the solar diurnal variations. Those kinds of data present gaps in records and consequently we explore them via a time-frequency gapped wavelet algorithm. We propose a new approach to analyze magnetograms based on scale correlation. The results show that the magnetic records have a latitudinal dependence affected by the season of year and by the level of solar activity. We have found a disparity on the latitudinal response at Southern and Northern Hemispheres during solstices, which is expected due to the asymmetry of the Sq field. On the other hand at equinoxes, records from stations located at approximately the same latitude but at different longitudes presented peculiar dissimilarities. The achieved results suggest that quiet day patterns and the physical processes involved in their formation are strongly affected by: the conductivity of the E-region, the geomagnetic field intensity and its configuration, and the thermospheric winds.

Keywords: Magnetogram data, Quiet days, Gapped Wavelet analysis, Wavelet Cross-correlation.

1. Introduction

The daily variations of the geomagnetic field were discovered by the English researchers Graham and Watchmaker (1724) through the observation of a compass needle motions in 1722. Since then, it is well known that a typical spectrum of those magnetic variations is composed by a few harmonics of the 24-h period (12, 8 and 6-h). They are described as “quiet daily geomagnetic field variations” - referred to as “Sq” for “solar quiet” field (Campbell, 1989).

The traditional method of calculating the baseline for the quiet day variations is to use the five quietest days for each month for each magnetic observatory. In this work, we propose a new approach to study quiet periods by eliminating the disturbed days using a multi-scale process. To accomplish this task, we study the harmonics of the solar diurnal variations using hourly data of the H component and explore it via a gapped wavelet technique based on the continuous wavelet transform (described in Frick et al., 1997, 1998). The gapped wavelet technique is suitable for analysis of data with gaps.

Originally continuous wavelet transforms (CWT) were applied in geophysics to analyze seismic signals in the pioneer works of Morlet (1983) and Grossmann and Morlet (1984). Nowadays,

16 the use of the wavelet technique has exponentially grown in many different areas (Farge , 1992).
17 A similar trend is noted in the application of the wavelet cross-correlation technique, which
18 has been used by many researchers, see for instance Frick et al. (2001); Oczeretko et al. (2006);
19 Rehman and Siddiqi (2009) and the pioneer work of Nesme-Ribes et al. (1995).

20 This work aims mainly to highlight and interpret the solar diurnal variations at a Brazilian
21 station compared to the observations at other twelve magnetic stations reasonably well distributed
22 over the whole Earth's surface. By applying gapped wavelet transforms to these signals, we
23 were able to analyze both the frequency content of each signal and the time dependence of
24 that content. After computing the wavelet transform, we performed wavelet cross-correlation
25 analysis, which was useful to isolate the period of geomagnetic spectral components in each
26 station and to correlate them as function of scale (pseudo-period or central-period).

27 The paper is organized as follows: Section 2 is devoted to explaining the principal mech-
28 anisms and aspects of the solar magnetic variations. Section 3, the analyzed period and data
29 are presented. Section 4 describes, divided in subsections, the used methodology: Section 4.1
30 presents a brief description of continuous wavelet transforms, Section 4.2 is devoted to introduce
31 the gapped wavelet analysis, and Section 4.3 to establish the wavelet cross-correlations and to
32 explain how they can be quantified. Section 5, the results are discussed and, Section 6 brings the
33 conclusions of this work. The paper also includes two appendixes which we present some CWT
34 application and mathematical details concerning to this work.

35 2. The Physics of the Solar Magnetic Variation

36 The major driving force for quiet day field changes seems to arise from the dynamo-current
37 process in the ionospheric E region between 90 and 130 km (Stewart, 1882). Tidal winds move
38 the ions across the Earth's magnetic field producing electro-magnetic forces (emfs). Those emfs
39 drive electric currents in the conducting E region which give rise to daily variations in the mag-
40 netic field measured at the ground level (for details see Chapman and Bartels, 1940). Through
41 these mechanisms, two vortices of currents are induced, one in the northern Hemisphere (clock-
42 wise) and another in the southern Hemisphere (counterclockwise). At the same time, a strong
43 eastward electric jet is formed throughout the equatorial region.

44 There are three factors that affect the dynamo process: the ionospheric wind, the ionospheric
45 conductivity and the geomagnetic field configuration. The wind and the conductivity vary sea-
46 sonally due to their dependence on the solar zenith angle (Campbell, 1989). Zhao et al. (2008)
47 concluded that the correlation between the Sq amplitude and solar zenith was higher in high
48 latitude than in low latitude regions due to the effect of the prenoon-postnoon asymmetry of Sq.

49 The Sq field variation has a main spatial dependence on latitude and is affected by other fac-
50 tors including epoch of the year and level of solar activity. Chapman and Stagg (1929) observed
51 two kinds of regular changes in the solar diurnal magnetic variations on quiet days: annual vari-
52 ation, that affects both the type and the amplitude during each year; and solar activity variation,
53 that affects fundamentally the amplitude along each sunspot cycle. Takeda (1999) estimated that
54 the intensity of the Sq currents in high solar activity was about twice larger than in low solar
55 activity.

56 Many other researchers studied the variations of the Sq, including Hibberd (1985) that exam-
57 ined the annual, semi-annual and even the whole solar cycle. Stening (1971) examined seasonal
58 variations and longitudinal inequalities of the electrostatic-field in the ionosphere by looking at
59 its electric conductivity and the Earth's main magnetic field. Takeda (2002) showed solar activity

60 dependence of the Sq amplitude, and explained this effect through the ionospheric conductivity.
61 Takeda (2002) also compared the amplitude of the Sq for the same value of conductivity. The
62 seasonal variation is seemingly due to differences in neutral winds or to the magnetic effect of the
63 field-aligned current (FAC) flowing between the two Hemispheres generated by the asymmetry
64 in the dynamo action. The FACs are controlled by interplanetary magnetic fields (IMF) and its
65 electric fields can directly penetrate to the equatorial ionosphere (Sastri, 1988).

66 Some evidence of the influence of oceanic tides on the magnetic daily variation has been
67 obtained by Larsen and Cox (1966). They found small semidiurnal variations of the Z component
68 at a coastal site (Cambria, California) and at two island stations (Honolulu and San Miguel) that
69 could not be explained by the atmospheric tidal theory. They suggested that these variations
70 must be due predominantly to oceanic tides. It is important to mention here that the conductivity
71 of the ocean does not vary significantly with time, unlike the ionospheric conductivity. As a
72 consequence, the seasonal variation of the oceanic contribution is expected to be smaller than the
73 ionospheric contribution (Cueto et al., 2003).

74 Magnetic stations on islands or coastlines are fully exposed to anomalous effects of the ocean
75 (Schmucker, 1999a,b). The oceans, as well as the ionosphere, constitute electrical conductors
76 and they are subject to tidal motions. As a result of the tidal flow of the ocean water, we might
77 expect the effects of some kind of dynamo (Parkinson, 1983). The electric current system induced
78 by the oceanic tides due to the drifting motion produces daily variation on magnetic stations
79 located at oceanic islands and nearby shores. Caution must be taken when interpreting the solar
80 magnetic variations at a particular station, if the purpose is to obtain a world-wide analysis of the
81 Sq field.

82 The total variation measured on the ground consists both of external (ionospheric current) and
83 internal (induced Earth current) contributions (Forbes and Lindzen, 1976). The pattern of the
84 conductivity of surfaces layers of the Earth will introduce a corresponding small scale pattern
85 into the distribution of the induced currents. At some stations, an accurate indication of the
86 average induced current system is difficult to determine, consequently its effects cannot be fully
87 distinguished (Price, 1969).

88 In his review, Price (1969) suggested that the interpretation of field variations at a particular
89 observatory must be done carefully. Although the ionosphere current system may have a fairly
90 simple world-wide pattern, the relatively small variation of the conductivity distribution of the
91 Earth's surface will introduce a corresponding small variation into the distribution of the induced
92 currents. However, the external origin contribution of the Sq field is about 2.5 times that of the
93 internal origin (Matsushita and Maeda, 1965). Therefore, in this work, we have disregarded the
94 influence of the internal contributions on the analysis of the diurnal geomagnetic variations.

95 **3. Magnetic Data**

96 In this section, we first describe the data used to study the quiet day variations. We also
97 discuss the considerations used in data treatment for the different magnetic stations.

98 *3.1. Dataset*

99 Our primary interest is to correlate the response of the geomagnetic field at Vassouras to the
100 other twelve previously chosen magnetic stations. The Vassouras Magnetic Observatory, is lo-
101 cated in Rio de Janeiro, Brazil, under the South Atlantic Magnetic Anomaly (SAMA) influence.
102 It has been active since 1915 and is a member of the INTERMAGNET program. One of the pe-
103 culiarities of VSS is its location, at low latitude, where the H component is essentially the same

104 as the total geomagnetic field. In forthcoming years, a Brazilian network of magnetometers will
105 be implemented and VSS could be used as reference.

106 To fulfill our purpose, we use hourly mean value series of the H geomagnetic component.
107 Some magnetic stations have available the X component, then we convert the X component of
108 XYZ system to the H component of the HDZ system of vector representation of the Earth's
109 magnetic field (as described in Campbell, 1989). We use $X = H \cos(D)$, where X is the vertical
110 component in the XYZ system, H is the horizontal magnitude and D is the angular direction
111 of the horizontal component from the geographic north (declination). In principle, this system
112 conversion does not affect our results because we only use magnetic stations of low- and mid-
113 latitudes and we are interested in the magnetic variations.

114 The magnetic stations that use the XYZ system are AMS, ASP, BEL and CLF. The conversion
115 of systems was performed for BOU, CMO, EYR, HON and SJG for the data between 1999 and
116 2003 and in BMT and KAK for the data between 1999 and 2004.

117 The distribution of the magnetic stations, with their IAGA code, is given in Fig. 1. The
118 corresponding codes and locations are given in Table 1 which the sequence is organized by
119 the geographical latitude of the stations. This work relies on data collections provided by the
120 INTERMAGNET programme (<http://www.intermagnet.org>).

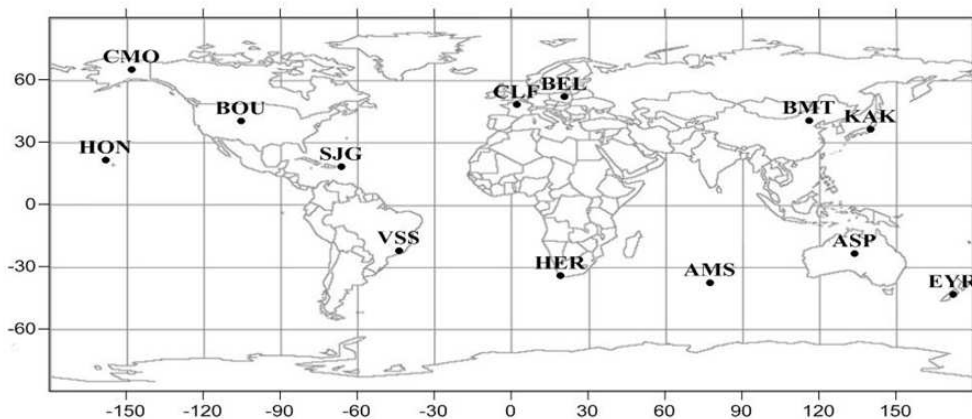


Figure 1: Geographical localization of the stations used in this work and their respective IAGA code.

121 We choose the period of geomagnetically quiet days to study seasonal and solar activity
122 variation. The data interval used in this work is from 1999 to 2007, almost the whole solar cycle
123 23 using the available dataset. In this data interval, the higher solar activity occurred between
124 2000 and 2001; and the lower solar activity, between 2005 and 2007. For seasonal variation
125 analysis, one year is divided into two seasons: solstices (June and December) and equinoxes
126 (March and September).

127 As a geomagnetic disturbance index, the Kp index has been chosen to distinguish the dis-
128 turbed days ($Kp > 3+$) from the quiet days ($Kp \leq 3+$). The global Kp index is a number
129 from 0 to 9 obtained as the mean value of the disturbance levels within 3-h interval observed at
130 13 subauroral magnetic stations (see Bartels, 1957). In our approach, the disturbed periods are
131 eliminated and considered as gaps. Therefore, in principle only the magnetic effects of the lunar
132 and solar contribution remained in the magnetic records.

Table 1: INTERMAGNET network of geomagnetic stations used in this study.

Station	IAGA code	Geographic coord.		Geomagnetic coord.	
		Lat.($^{\circ}$)	Long.($^{\circ}$)	Lat.($^{\circ}$)	Long.($^{\circ}$)
Eyrewell (New Zealand)	EYR	-43.42	172.35	-46.79	-106.06
Martin de Vivies (France)	AMS	-37.83	77.56	-46.07	144.94
Hermanus (South Africa)	HER	-34.41	19.23	-33.89	84.68
Alice Springs (Australia)	ASP	-23.76	133.88	-32.50	-151.45
Vassouras (Brazil)	VSS	-22.40	-43.65	-13.43	27.06
San Juan (Puerto Rico)	SJG	18.12	-66.15	27.93	6.53
Honolulu (United States)	HON	21.32	-158.00	21.59	-89.70
Kakioka (Japan)	KAK	36.23	140.18	27.46	-150.78
Boulder (United States)	BOU	40.13	-105.23	48.05	-38.67
Beijing (China)	BMT	40.30	116.20	30.22	-172.55
Chambon la Foret (France)	CLF	48.02	2.26	49.56	85.72
Belsk (Poland)	BEL	51.83	20.80	50.05	105.18
College (United States)	CMO	64.87	-147.86	65.36	-97.23

Source: <http://wdc.kugi.kyoto-u.ac.jp/igrf/gggm/index.html> (2010)

133 3.2. Data Treatment Considerations

134 As previously mentioned, we are focusing the study of VSS responses to Sq variations, particularly, its diurnal and semidiurnal period spectral components. As VSS is located at low
135 latitude, the majority of magnetic stations used here are spread between low- and mid-latitudes.
136 We only use one magnetic station (CMO) located at high latitude for comparison. In the polar
137 region, disturbance events have been included because there were not enough truly quiet days
138 with our Kp selection ($Kp \leq 3+$). Above 60° , magnetospheric processes may completely dominate the magnetic recordings what impedes the Sq observation (Campbell, 1989). At low- and
139 mid-latitude, the magnetograms should be not seriously affected by auroral electrojet and the Sq
140 currents would correspond to regularly recurring phenomena (Price, 1969).
141

142 The Sq variations were greatly explored over the last decades, as well as their spatial dependence on latitude and others factors, including epoch of the year and level of solar activity (Price, 1969; Stening, 1971; Hibberd, 1985; Campbell, 1997; Le Sager and Huang, 2002; Takeda, 2002).
143

144 We take into consideration the two well known facts about the Sq field cited by Price (1969):
145

- 147 1. It is largely a local time field that can be roughly represented by a current fixed to the Sun,
148 then we use the data at Universal Time (UT) to observe the global variance of the Sq field.
- 149 2. It is influenced by the Earth's main field throughout the latitudes between 60° N and 60° S,
150 then we do not use magnetic stations of high latitudes (auroral zone), except CMO.

151 On one hand, at high and polar latitudes, the geomagnetic field lines are aligned almost vertically then the ionospheric currents are joined with the field-aligned currents (FAC), and
152 the electrodynamics is dominated by the influence of the solar-wind-magnetosphere interaction processes (Yomoto, 2006). On the other hand, the ionospheric current at middle and low latitude
153 is generated by the influence of tidal winds, *i.e.*, ionospheric wind dynamo (Sastri, 1988).
154

155 An adequate knowledge of the daily variation field and a full understanding of the associated phenomena can only come from extensive and detailed analysis of the mean hourly values of the
156
157

158 magnetic elements at many stations (Price, 1969). Therefore, the availability of these data in the
 159 World Data Centers that collect and distribute these data is of enormous help.

160 4. Methodology

161 The method used in this study is based on continuous wavelet transforms. In this section, we
 162 first introduce the concepts of the CWT and its properties. Following, we introduce the gapped
 163 wavelet analysis and emphasize its improvements over the CWT. After that, we describe how we
 164 extract the information of the observed data using wavelet cross-correlation analysis.

165 4.1. Continuous Wavelet Transform

166 The wavelet transform was introduced at the beginning of the 80s of the XX century by
 167 Morlet (1983), who used it to study seismic data. Grossmann and Morlet (1984) improved the
 168 windowed Fourier transform and they constructed the continuous wavelet transform (CWT). The
 169 idea was to change the width of the window function accordingly to the frequency of the signal
 170 being considered. The CWT is an integral transform, and it yields an affine invariant time-
 171 frequency representation. A wavelet transform can measure the time evolution of the frequency
 172 transients within the signal. In this transform, we use as basis a set of functions called wavelets.

173 Formally, in order to be called wavelet, a function ψ must satisfy some conditions. First, the
 174 admissibility condition which is usually related to the mean zero of the wavelet function,

$$\int \psi(t) dt = 0. \quad (1)$$

175 Second, the wavelet function should be localized with compact or effective compact support.
 176 The CWT of a time series f is defined by the integral transform,

$$W(a, b) = \int f(t) \frac{1}{\sqrt{a}} \psi^* \left(\frac{t-b}{a} \right) dt, \quad a > 0, a \in \mathbb{R}, \quad (2)$$

177 where $*$ represent the complex conjugate and the pre-factor $|a|^{\frac{1}{2}}$ is introduced in order to guar-
 178 antee that all the scaled functions $|a|^{\frac{1}{2}} \psi(\frac{t}{a})$, have the same energy in $\mathbb{L}^2(\mathbb{R})$ sense. This function
 179 $W(a, b)$ represents the wavelet coefficients that is a function of both time and frequency (time b
 180 and scale a).

181 There are many possible kinds of wavelets. The choice of wavelets depends both on the data
 182 and the analysis objectives (Domingues et al., 2005, and references therein). Therefore, there is
 183 no best wavelet for signal analysis in general. In this case, we use the Morlet wavelet function
 184 that represents well the signals we are analyzing.

185 It is possible to analyze a signal in a time-scale plane. In the wavelet analysis it is called
 186 the wavelet scalogram. In analogy with the Fourier analysis, the square modulus of the wavelet
 187 coefficient $|W(a, b)|^2$ is used to provide the energy distribution in the time-scale plane. In the
 188 wavelet analysis, we can also explore the central frequencies ε_ψ (or central periods $\frac{1}{\varepsilon_\psi}$) of the
 189 time series through the global wavelet spectrum, also called pseudo-frequencies ε_a (or pseudo-
 190 periods),

$$\varepsilon_a = \frac{\varepsilon_\psi}{a \Delta t}. \quad (3)$$

191 where Δt is the sampling period (Abry, 1997).

192 It helps to understand the behavior of the energy at a certain scale.

193 4.2. Gapped Wavelet Analysis

194 Magnetograms are finite length observational data series and may contain gaps of various
 195 sizes. To reduce gap problems, we use the gapped wavelet analysis a technique introduced by
 196 Frick et al. (1997) and afterwards improved in Frick et al. (1998). In this transform, the admissi-
 197 bility condition is broken when the wavelet overlaps data gaps. The leading idea of the gapped
 198 technique is to restore the admissibility condition by repairing in some way the wavelet itself.

199 Considering the function $f(t)$ is only known in some intervals of time and it can be rewritten
 200 as

$$f'(t) = f(t) G(t) \quad (4)$$

201 where $G(t)$ is the function of data gaps, which is equal to 1 if the signal is registered and is equal
 202 to zero otherwise, therefore, the analyzing wavelet became

$$\psi'_{a,b}(t) = \frac{1}{\sqrt{a}} \psi\left(\frac{t-b}{a}\right) G(t). \quad (5)$$

203 Near a gap, the function ψ' is used instead of the base wavelet ψ , and consequently, ψ' will no
 204 longer satisfy the admissibility condition (Equation 1). The function G transfers the gap problem
 205 from the signal $f(t)$ to the broken wavelet ψ' , which will be replaced by an adaptive wavelet $\tilde{\psi}$ in
 206 order to satisfy the admissibility condition.

207 To restore the admissibility condition, the analyzing wavelet ψ can be considered to be in the
 208 form

$$\psi(t) = h(t) \varphi(t), \quad (6)$$

209 where $h(t)$ is the oscillatory part and $\varphi(t)$ is the envelope.

210 In this analysis, we use the Morlet wavelet,

$$\psi(t) = \exp\left(\frac{-t^2}{2\sigma^2}\right) \exp(i\omega_0 t), \quad (7)$$

211 with $\iota = \sqrt{-1}$, $\omega_0 = 6$ and $\sigma = 1$, σ is the time resolution parameter. Using Morlet wavelet with
 212 $\omega_0 = 6$ gives a value of $\varepsilon_\psi = 0.9709$ and Fourier period, T , equal to $T = 1.03 a$, where a is the
 213 scale. It indicates, that for the Morlet wavelet, the scale is approximately equal to the Fourier
 214 period (see Farge , 1992; Abry, 1997; Torrence and Compo , 1998, for more details).

215 The adjustable parameter σ gives the optimal time-frequency resolution. Small values of
 216 σ give better time resolution, while large values improve frequency resolution. In the gapped
 217 wavelet case, the problem of the admissibility condition breaks down when σ is below 1. It must
 218 be avoided. However, a wide range of σ can be used. The choice of σ is highly restricted by
 219 the admissibility condition, because there are not enough oscillations to give a zero in average.
 220 However, the gapped technique corrects the wavelet in this case as well and nullifies the mean.
 221 Thus this problem is completely resolved by the gapped technique (Soon et al., 1999). For more
 222 details see Appendix A.

223 Following Frick et al. (1997), we use Morlet wavelet where

$$h(t) = \exp(i\omega_0 t), \quad (8)$$

224

$$\varphi(t) = \exp\left(\frac{-t^2}{2\sigma^2}\right). \quad (9)$$

225 When the wavelet is disturbed by the gap, we can restore the admissibility condition by
226 including a function $K(a, b)$ in the oscillatory part of the wavelet,

$$\tilde{\psi}(t, b, a) = \left[h\left(\frac{t-b}{a}\right) - K(a, b) \right] \varphi\left(\frac{t-b}{a}\right) G(t) \quad (10)$$

227 and requiring,

$$\int \tilde{\psi}(t) dt = 0. \quad (11)$$

228 The introduced function $K(a, b)$ can be determined for each scale a and position b from (10)
229 and (11), and could be obtained as

$$K(a, b) = \left[\int \varphi\left(\frac{t-b}{a}\right) G(t) dt \right]^{-1} \left[\int h\left(\frac{t-b}{a}\right) \varphi\left(\frac{t-b}{a}\right) G(t) dt \right]. \quad (12)$$

230 It was shown that this technique not only suppresses the noise caused by the gaps and bound-
231 aries, but improves the accuracy of frequency determination of short or strongly gapped signals.

232 In summary, the advantages of the CWT using gapped wavelet in comparison with the use of
233 the traditional CWT are:

234

- 235 1. The gapped wavelet technique helps to reduce the effects of two problems of the detection
236 of periodicities in times series: the presence of gaps in time series and boundary effects
237 due to the finite length of time series.
- 238 2. The method involves a correction of the analyzing wavelet to fulfill the admissibility con-
239 dition and is independent of a particular choice of analyzing wavelet.
- 240 3. This technique not only suppresses the low and high noise frequencies, but it is also better
241 at estimating the frequency of the signal.

242 In Appendix B, we present an example of the gapped wavelet use in a synthetic signal.

243 4.3. Wavelet Cross-correlation Analysis

244 The approach of this work is to use the wavelet cross-correlation, $C(a)$, to study the cor-
245 relation between a pair of magnetic data from different stations as a function of scale (see
246 Nesme-Ribes et al. (1995) and Frick et al. (2001) for more mathematical details):

$$C(a) = \frac{\int \mathcal{W}_1(a, t) \mathcal{W}_2^*(a, t) dt}{\left(\int \mathcal{W}_1(a, t)^2 dt \int \mathcal{W}_2(a, t)^2 dt \right)^{\frac{1}{2}}} \quad (13)$$

247 where $\mathcal{W}_i(a, t) = |W_i(a, t)| - \overline{|W_i(a, t)|}$, W_i are the wavelet coefficients and $\overline{W_i}$ is the arithmetic
248 mean in time for $i = 1$ or 2 . We can also obtain the determination coefficient, $D(a)$, as function
249 of the scale a . It is defined as the square of the correlation coefficient,

$$D(a) = C(a)^2. \quad (14)$$

250 One of the reasons to use the coefficient of determination instead of the correlation is to
251 compute the statistics in order to determine the size or magnitude of the relation between two
252 variables. It is interpreted as the percentage of variability of the response variable explained by
253 the regression model. The correlation coefficient measures linear association. Though in space
254 geophysics both the determination and correlation coefficient are used (Reiff, 1983). In our case,
255 we prefer to use the determination coefficient due to its interpretation of linear regression.

256 As mentioned above, in the wavelet representation, each scale (a) explains part of the distri-
257 bution of energy of the whole signal through time. The wavelet cross-correlation allows us to
258 check the interaction between two sets of data for each considered scale. The scales are chosen
259 in such a way that they make possible to characterize the dominating periods in the geomagnetic
260 data spectrum. In our case, we choose the scales which correspond to the periods of 24 and 12
261 hours, related to the diurnal magnetic variations.

262 5. Results and Discussion

263 Fig. 2 and Fig. 3 show the interpretation of the CWT and the CWT using gapped wavelet
264 techniques, with the purpose highlighting the reasons to use gapped wavelet techniques over the
265 CWT to study quiet days. Fig. 2 shows an example of CWT applied to a real signal, in this case,
266 a magnetogram data. In this analysis, as function of time, $f(t)$, we use the H component obtained
267 in June, 2007 at VSS station. Fig. 2 shows: (a) the H component, (b) the wavelet square modulus
268 (scalogram) and (c) the global wavelet spectrum (total energy in each scale). In the scalogram,
269 areas of stronger wavelet power are shown in dark red on a plot of time (horizontally) and time
270 scale (vertically). The areas of low wavelet power are shown in dark blue. It is possible to notice
271 a maximum of wavelet power on the scalogram and, also on the global wavelet spectrum, at the
272 time scale corresponding to 24-h period, and a less pronounced second peak at the time scale
273 corresponding to 12-h period. The scalogram shows also the cone of influence, region where
274 edge effects become important and the wavelet coefficients are not reliable.

275 Magnetograms may contain gaps of various sizes. Here, we also added gaps due to the
276 removal of the disturbed days. These disturbed days were removed before the gapped wavelet
277 transform was performed. In our case, the gapped wavelet technique helps to reduce the effects
278 due to the presence of gaps and also boundary effects due to the finite length of data. The gapped
279 wavelet (used and validated on the synthetic signal - Appendix B) was then applied in real data
280 as shown in Fig. 3. One might notice that Fig. 3 is very similar to Fig. 2, the difference is that
281 now we introduced gaps due to disturbed days. As our interest is only to study the quiet day
282 variations, we consider the disturbed days (where $Kp > 3+$) as gaps. Even with the additional
283 gaps, the global wavelet spectrum, Fig. 3(c), still shows a pronounced increase of energy in the
284 24-h and a less dominant in the 12-h period. In the scalogram, the 24-h period shown in dark red
285 is clearly visible and the 12-h period in the reddish color appears less dominantly compared to
286 the 24-h. Also, it is not necessary to include the cone of influence, because the gapped wavelet
287 technique not only suppresses the boundary and gaps in both high and low frequencies, but also
288 estimates better the frequency of the signal (see Frick et al. (1998)). Comparing Fig. 2 and Fig. 3,
289 there is not a significant difference in the common intervals of the CWT and gapped scalograms.
290 The inclusion of gaps in the data due to the removal of the disturbed days does not affect the
291 analysis of the diurnal and semidiurnal variations.

292 With the gapped wavelet coefficients in hand, we exclude the coefficients that corresponded
293 to the gaps areas in the scalograms. The excluded areas are presented as white rectangles in
294 Fig. 3. It is an artificial lack of data that follows the methodology established in Appendix A

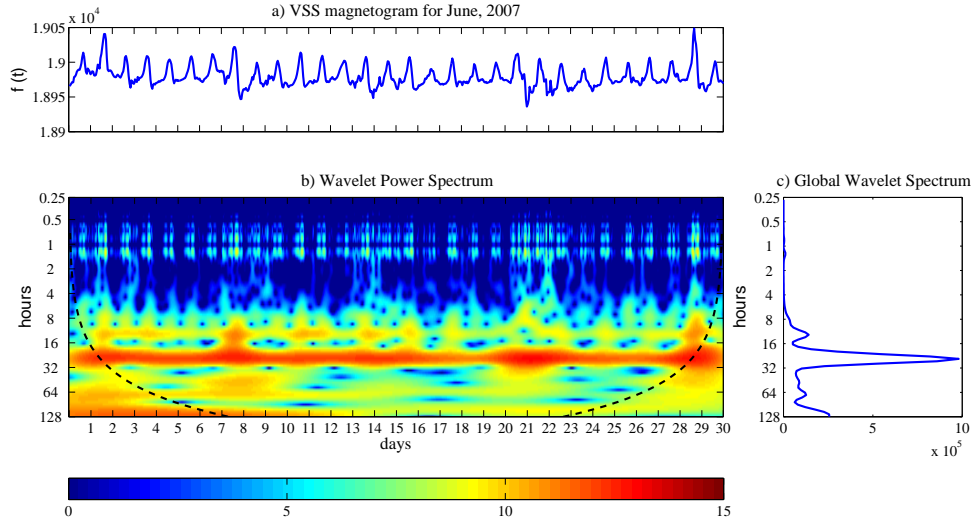


Figure 2: Example of CWT application to a real signal: (a) H component of VSS at June, 2007 used for the wavelet analysis, (b) the scalogram using Morlet wavelet, logarithmic scaled representing $\log_2(|W(a,b)|)$ and (c) the global wavelet spectrum.

295 (which it has purpose to highlight the gapped wavelet property of the estimating frequency of the
 296 signal in the gaps regions similar to an interpolation method), so Fig. 3 highlights the wavelet
 297 coefficients excluded before performing the cross-correlation wavelet analysis. Because we are
 298 only interested in the quiet-days behavior analysis.

299 This methodology structures a new way of dealing with daily magnetic variation for quiet
 300 periods.

301 The same procedure of excluding the disturbed days and consider them as gaps is performed
 302 for the whole dataset used in this study. Also, after the gapped wavelet transform, we have
 303 also excluded all the wavelet coefficients that corresponded to these gaps in the scalograms.
 304 Therefore, the cross-correlation wavelet analysis were done only using the wavelet coefficients
 305 that corresponded to the quiet days.

306 After excluding all the wavelet coefficients that correspond to gaps, we have calculated the
 307 cross-correlation functions $C(a)$, for each pair formed by Vassouras and each one of the twelve
 308 chosen magnetic stations (see equation 13 for mathematical details). This procedure was done
 309 for the years 1999 to 2007 during the equinoxes and solstices. These calculations were performed
 310 in order to understand the global response of the Sq variation at different locations.

311 To exemplify the results obtained by calculating wavelet correlation, we selected the period
 312 of June, 2007. Fig. 4 shows the modulus of the correlations functions (for this period) for the
 313 twelve magnetic stations. The correlation graphics are displayed by magnetic stations from top
 314 to bottom and divided in two blocks, in alphabetic order. These selected stations can be divided
 315 as follows: low latitude (ASP, BMT, HER, HON, KAK and SJG), medium latitude (AMS, BEL,
 316 BOU, CLF and EYR) and high latitude (CMO). On the vertical axis, we present the correlation
 317 coefficients and in the horizontal axis, the scale (period in hours). The periods of 24, 12, 8 and
 318 6-h are highlighted with dashed lines in order to facilitate visual inspection and comparison. It
 319 is possible to verify that for most of the pairs $C(a)$ varies considerably with scale. We observe

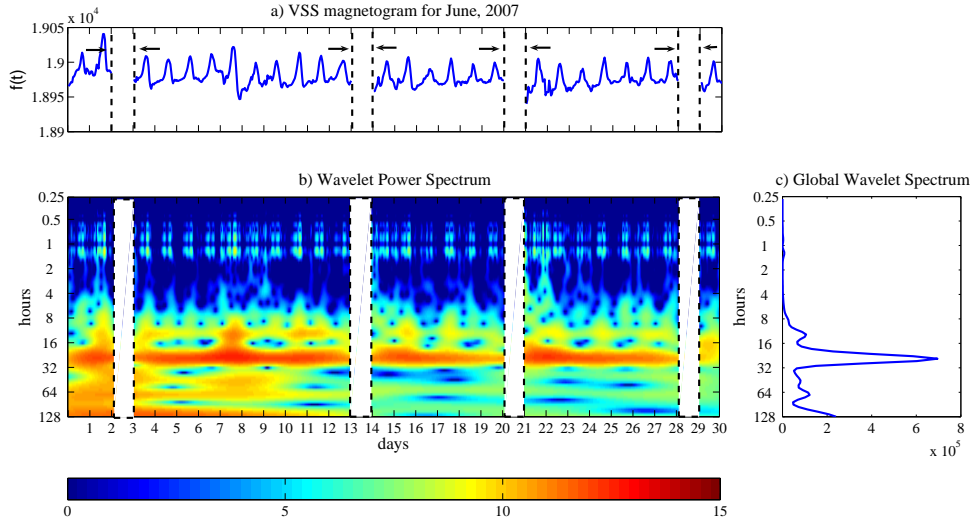


Figure 3: Example of application of gapped wavelets to a real signal with added gaps: (a) H component of VSS at June, 2007 with additional gaps due to the disturbed days; (b) the local wavelet power spectrum using Morlet wavelet, logarithmic scaled representing $\log_2(|W(a, b)|)$ and (c) the global wavelet spectrum.

320 that the correlation between two geomagnetic data sets is scale dependent. We also observe that
 321 the correlation is usually larger for the first harmonics of the diurnal variations, and it is smaller
 322 for the following harmonics.

323 The determination coefficients $D(a)$ were obtained by applying the equation 14 to the values
 324 of coefficients extracted from the wavelet correlation curves (see Fig. 4). Once we determined
 325 the correlation coefficients for 24 and 12-h periods, we were able to calculate the determination
 326 coefficients. In order to facilitate the analysis of the determination coefficients, we calculated
 327 the mean determination coefficient $\overline{D(a)}$ for three different periods corresponding to high solar
 328 activity (years of 1999, 2000 and 2001), medium solar activity (years of 2002, 2003 and 2004)
 329 and low solar activity (years of 2005, 2006 and 2007).

330 Fig. 5 and 6 show the mean determination coefficient for the 12 chosen stations during the
 331 equinoxes and solstices between the years of 1999 and 2007. These figures present the diurnal
 332 and semidiurnal geomagnetic variations, respectively, and their seasonal behavior. In the vertical
 333 axis, we present the determination coefficient and in the horizontal axis, the twelve chosen
 334 magnetic stations ordered by latitude from the Southern to the Northern Hemisphere. This distribu-
 335 tion of stations helps to verify the latitudinal dependence of the diurnal variations. The nine
 336 years interval enables the study of the solar activity dependence upon the Sq variations. Years
 337 of high solar activity are shown in black (corresponding to the mean value of the determination
 338 coefficient for the years of 1999, 2000 and 2001), years of medium solar activity, in grey (cor-
 339 responding to the mean value of the determination coefficient for the years of 2002, 2003 and 2004)
 340 and years of low solar activity, in white (corresponding to the mean value of the determination
 341 coefficient for the years of 2005, 2006 and 2007).

342 In Fig. 5, it is possible to identify a primary latitudinal dependence for the equinoxes and
 343 solstices. At equinoxes, the stations of AMS, ASP and HON have the largest values of the mean
 344 determination coefficients considering the three periods of analysis for March, and the stations

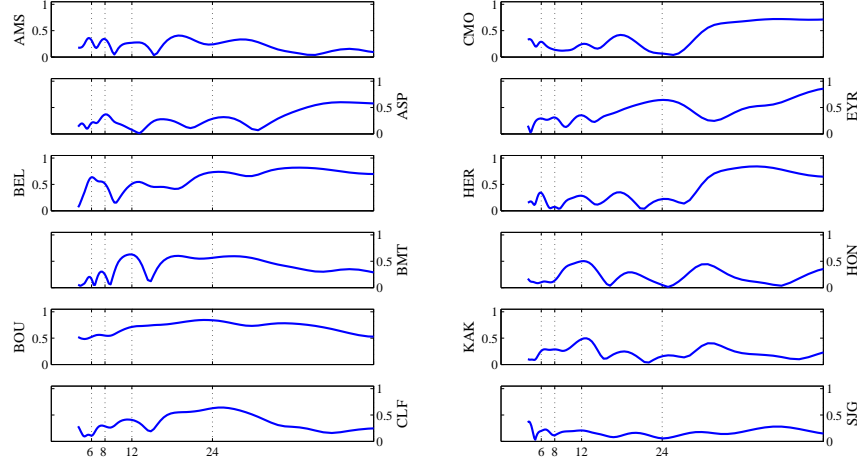


Figure 4: Modulus of the wavelet cross-correlation functions for each pair formed by VSS and one of the twelve chosen magnetic stations for June, 2007.

345 of AMS, HER and SJG, for September. If we consider the simple dipole representation of the
 346 Earth's main magnetic field and the north-south symmetry between Hemispheres of thermo-
 347 spheric wind and conductivity field in equinox conditions, we would find that the stations at the
 348 same latitude should have the same determination coefficient. The stations of EYR (located at
 349 Geomagnetic coord. Lat. 46.79°) and AMS (located at Geomagnetic coord. Lat. 46.07°), and of
 350 SJG (located at Geomagnetic coord. Lat. 27.93°) and KAK (located at Geomagnetic coord. Lat.
 351 27.46°) should have similar values of the mean determination coefficients at the equinoxes. By
 352 analyzing Fig. 5, this fact does not hold for the months of March and September. The geomag-
 353 netic field is asymmetric, thus, the mean conductance for the Northern and Southern Hemisphere
 354 will have different values even at equinox (Stening, 1971). This characteristic may explain the
 355 difference of response between the magnetic stations of EYR and AMS because they are located
 356 at similar magnetic latitudes but at different Hemispheres. However, this does not explain the dif-
 357 ference of response between the magnetic stations of SJG and KAK. Also, the stations of EYR,
 358 AMS, ASP, HON, SJG, BMT, KAK and BEL have largest values of the mean determination coef-
 359 ficients during the high and medium solar activity than during the low solar activity on March,
 360 and the stations of EYR, BMT, BOU, KAK, CLF, BEL and CMO, on September.

361 The disparity in the response of magnetic stations between solstices is expected. In Fig. 5, we
 362 expect low values of the mean determination coefficients between VSS and the magnetic stations
 363 located in the Northern Hemisphere (BEL, BMT, BOU, CMO, HON, KAK and SJG) as a result
 364 of the month of June and December be solstices, and consequently, of the wind asymmetry
 365 between the Northern and Southern Hemispheres due to the contrast in summer-winter radiation.
 366 Even so, latitudinal dependence prevailed at the solstices. The stations of HER, ASP, HON, SJG,
 367 CLF and BEL have the largest values of the mean determination coefficients considering the three
 368 periods of analysis for June. The stations HON, SJG, CLF and BEL located on the Northern
 369 Hemisphere presented larger mean determination coefficients which can be attributable to the

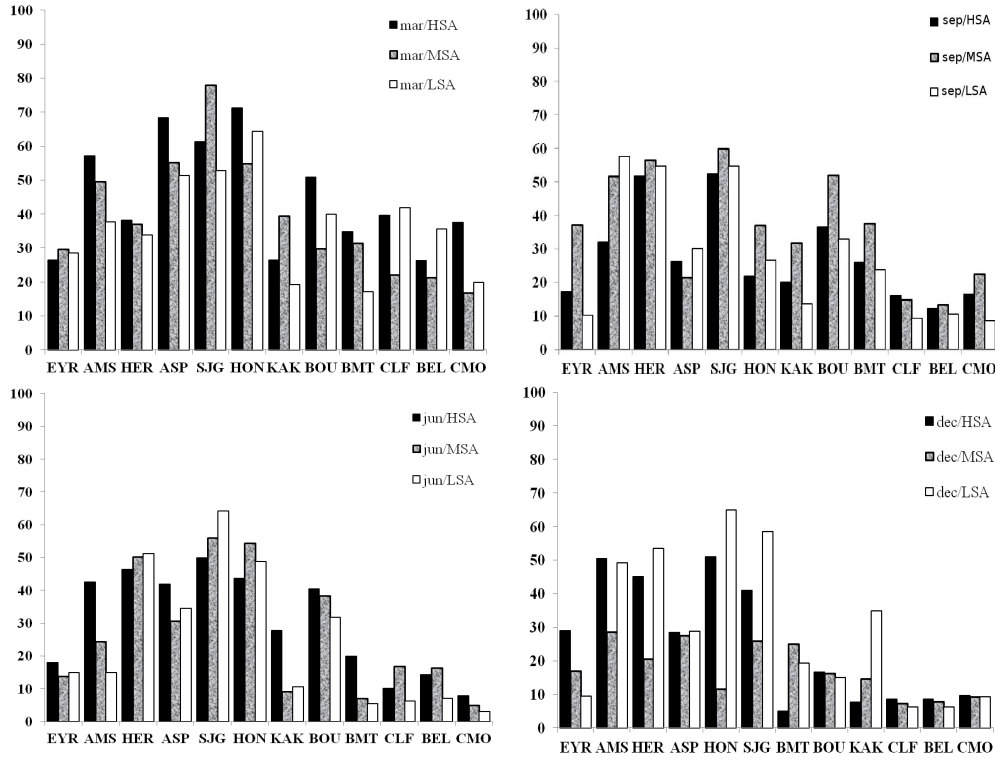


Figure 5: Bar graphs of the diurnal geomagnetic variation during the equinoxes (March and September) and solstices (June and December) months for three different periods corresponding to high solar activity shown in black (years of 1999, 2000 and 2001), medium solar activity shown in grey (years of 2002, 2003 and 2004) and low solar activity shown in white (years of 2005, 2006 and 2007). The vertical axis shows the mean of determination coefficient $\bar{D}(a)$ and the horizontal shows the IAGA code of the magnetic stations distributed from the lowest latitude on the South Hemisphere to the highest latitude on the North Hemisphere.

370 latitudinal dependence prevalence of the Sq current over the wind asymmetry. The largest values
 371 for December are not as perceptible as for the other months. Also, the stations of HER, ASP and
 372 SJG have largest values of the mean determination coefficients during the medium and low solar
 373 activity than during the high solar activity on June, and the stations of BMT, KAK, CLF and
 374 BEL, on December. This characteristic may be explained by the thermosphere wind asymmetry
 375 during the minimum solar activity which is not as larger as during the maximum solar activity.
 376 Magnetic stations of HER, HON and SJG located at lower latitudes as VSS usually present larger
 377 mean determination coefficients. These differences in responses between the stations located at
 378 similar latitudes as EYR and AMS, HER and ASP, SJG and KAK and BOU and CLF can be
 379 explained by the following features of the Sq field reported by Matsushita and Maeda (1965): 1)
 380 the total Sq current intensity is about 1.5 times larger in the Hemisphere's summer than in the
 381 winter and 2) the latitudinal position of the external current center is higher in summer than in
 382 winter.

383 In this work, we also find that the 24-h diurnal variation presented differences values of the
 384 mean determination coefficient for magnetic stations located in approximately the same geomag-
 385 netic latitude (EYR and AMS, HER and ASP, SJG and KAK, and BOU and CLF) but different

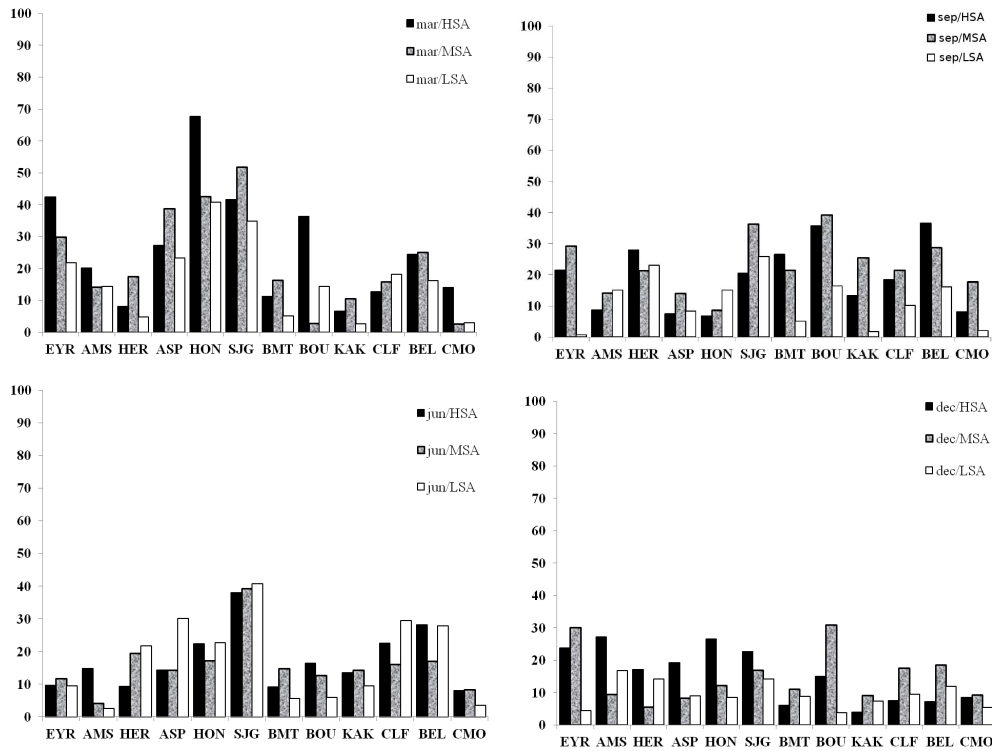


Figure 6: Bar graphs of the semidiurnal geomagnetic variation during the equinoxes (March and September) and solstices (June and December) months for three different periods corresponding to high solar activity shown in black (years of 1999, 2000 and 2001), medium solar activity shown in grey (years of 2002, 2003 and 2004) and low solar activity shown in white (years of 2005, 2006 and 2007). The vertical axis shows the mean of determination coefficient $\overline{D}(a)$ and the horizontal shows the IAGA code of the magnetic stations distributed from the lowest latitude on the South Hemisphere to the highest latitude on the North Hemisphere.

386 longitudes. This means that these stations are affected differently by the E-layer dynamo. At
 387 equinoxes, the mean determination coefficient was usually larger in years of higher solar activity,
 388 and at solstices it is practically larger in the year of lower solar activity. These results may be
 389 explained by the variation of conductivity of the E-region which has an ionization density de-
 390 pendency (Forbes and Lindzen, 1976). Also, the total geomagnetic field affects the conductivity
 391 through its dependence on electron and ions gyro-frequencies (Stening, 1971).

392 Another strong influence, very important to be referred, is the intensity of the geomagnetic
 393 field. The total geomagnetic field is particularly high in the regions of Central Canada, Siberia
 394 and South of Australia and it is quite low near Southern Brazil (Campbell, 1997). In Fig. 5, it is
 395 possible to observe that the magnetic stations, located at the Northwest of Canada (CMO), North
 396 of the United States (BOU), China (BMT), Japan (KAK) and Central Australia (ASP), where the
 397 geomagnetic field is particularly high, presented lower determination coefficient when compared
 398 to other stations.

399 For the semi-diurnal variation, the latitudinal dependence is not as perceptible as in the diur-
 400 nal variation (see Fig. 5 and 6). Also, the equinoxes and solstices present irregular distribution
 401 due to the solar activity.

402 A lower correlation between VSS and CMO is expected because CMO is a station located at
403 high latitude. In this region, the influence of the Sq currents is limited when compared to low and
404 mid-latitudes. At high latitudes, the major influence comes from a large horizontal current that
405 flows in the D and E regions of the auroral ionosphere, called the Auroral Electrojet. There are
406 two characteristic of the auroral region that we must mentioned. First of all, the conductivity in
407 the auroral ionosphere is generally larger than at lower latitudes. Second, the horizontal electric
408 field in the auroral ionosphere is also larger than at lower latitudes. Since the strength of the
409 current flow is directly proportional to the vector product of the conductivity and the horizontal
410 electric field, the auroral electrojet currents are generally larger if compared to those at lower
411 latitudes (see Sizova (2002) for more details).

412 6. Conclusions

413 A world-wide distribution of the harmonic components of solar diurnal variations (24 and 12-
414 h periods) has been observed in latitude and longitude by using the gapped wavelet analysis and
415 the wavelet cross-correlation technique. The objective of this paper is to study the characteristics
416 of these variations at a Brazilian station as compared to the features from other magnetic stations
417 to better understand the dynamics of the diurnal variations involved in the monitoring of the
418 Earth's magnetic field. The main results in this analysis can be summarized as follows:

- 419 1. The stations of EYR (Geomagnetic coord. Lat. 46.79°) and AMS (Geomagnetic coord.
420 Lat. 46.07°); and of SJG (Geomagnetic coord. Lat. 27.93°) and KAK (Geomagnetic
421 coord. Lat. 27.46°) located at similar latitudes presented very different values of the mean
422 determination coefficients at the equinoxes. This characteristic may be explained by the
423 difference in the mean conductance for the Northern and Southern Hemisphere due to the
424 asymmetry of the geomagnetic field.
- 425 2. At equinoxes and solstices, magnetic stations located at the Northwest of Canada (CMO),
426 North of the United States (BOU), China (BMT), Japan (KAK) and Central Australia
427 (ASP), where the geomagnetic field is particularly high, presented lower mean determina-
428 tion coefficient when compared to other stations. This fact can be explained by the peculiar
429 location of the VSS, under the South Atlantic Magnetic Anomaly (minimum geomagnetic
430 field intensity).
- 431 3. For the diurnal variation, the determination coefficient was usually larger in years of higher
432 solar activity at the equinoxes. The dependence of the E-region conductivity on the ion-
433 ization density may explain the variation of the mean determination coefficient due to the
434 solar activity.
- 435 4. The 24-h diurnal variation presented different values of the mean determination coefficient
436 for magnetic stations located in approximately the same geomagnetic latitude (EYR and
437 AMS; HER and ASP; SJG and KAK; and BOU and CLF) but different longitudes. The
438 anisotropy of the E-region electric conductivity because of the effect of the geomagnetic
439 field also may account for the differences of the mean determination coefficient among
440 these stations.
- 441 5. The latitudinal dependence for the semi-diurnal variation was not as noticeable as for the
442 diurnal variation, and also, presented an irregular distribution due to the solar activity.

443 6. In closing, this analysis has shown a great spatial and temporal variability of the diurnal
444 and semidiurnal variations, and also, unequal contributions for each station according to
445 their correlation to VSS due to the conductivity of the E-region, the geomagnetic field
446 intensity and its configuration, and thermospheric winds.

447 The gapped wavelet analysis is an alternative technique to study data series that contain gaps
448 of various sizes. Consequently, as proposed here, it can be used to exclude disturbed days and
449 to study the characteristics of solar diurnal variations. Using a network of magnetic stations, we
450 determine the contributions of the longitude and latitude and also of the total geomagnetic field.

451 7. Acknowledgments

452 V. Klausner wishes to thanks CAPES for the financial support of her PhD (CAPES – grants
453 465/2008) and her Postdoctoral research (FAPESP – 2011/20588-7). This work was supported
454 by CNPq (grants 309017/2007-6, 486165/2006-0, 308680/2007-3, 478707/2003, 477819/2003-
455 6, 382465/01-6), FAPESP (grants 2007/07723-7) and CAPES (grants 86/2010-29, 0880/08-6,
456 86/2010-29, 551006/2011-0, 17002/2012-8). Also, the authors would like to thank the INTER-
457 MAGNET programme for the datasets used in this work. The authors sincerely acknowledge a
458 reviewer whose comments and advices have greatly contributed to improve the final form of this
459 work

460 References

- 461 Abry, P., 1997. Ondelettes et turbulence. Multirésolutions, algorithmes de décomposition, invariance d'échelles; Diderot
462 Editeur:Paris.
- 463 Bartels, J., 1957. The technique of scaling indices k and q of geomagnetic activity. *Annals of the International Geophys-*
464 *ical Year* (4), 215–226.
- 465 Campbell, W. H., 1989. An introduction to quiet daily geomagnetic fields. *Pure and Applied Geophysics* 131 (3), 315–
466 331.
- 467 Campbell, W. H., 1997. *Introduction to Geomagnetic Fields*. Cambridge University Press, New York.
- 468 Chapman, S., Bartels, J., 1940. *Geomagnetism*. Oxford University Press, London.
- 469 Chapman, S., Stagg, J. M., 1929. On the variability of the quiet day diurnal magnetic variation at Eskdalemuir and
470 Greenwich. *Proceedings of the Royal Society London A* 123, 27–53.
- 471 Cueto, M., McKnight, D., Herraiz, M., 2003. Daily geomagnetic variations on the Iberian peninsula. *Geophysical Journal*
472 *International* 152 (1), 113–123.
- 473 Daubechies, I., Sep. 1990. The wavelet transform, time-frequency localization and signal analysis. *IEEE Transactions on*
474 *Information Theory* 36 (5), 961–1005.
- 475 Domingues, M. O., Mendes, O. J., Mendes da Costa, A., 2005. Wavelet techniques in atmospheric sciences. *Advances*
476 *in Space Research* 35 (5), 831–842.
- 477 Farge, M., 1992. Wavelet Transforms and their Applications to Turbulence. *Annual Reviews in Fluid Mechanics*, 24 (1),
478 395–458.
- 479 Forbes, J., Lindzen, R. S., 1976. Atmospheric solar tides and electrodynamics effects. i. the global sq current system.
480 *Journal of Atmospheric and Solar-Terrestrial Physics* 38, 897–910.
- 481 Frick, P., Baliunas, S. L., Galyagin, D., Sokoloff, D., Soon, W., 1997. Wavelet analysis of stellar chromospheric activity
482 variations. *The Astrophysical Journal* 483 (1), 426–434.
- 483 Frick, P., Beck, R., Berkhuijsen, E. M., Patrickeyev, I., 2001. Scaling and correlation analysis of galactic images. *Monthly*
484 *Notices of the Royal Astronomical Society* 327 (4), 1145–1157.
- 485 Frick, P., Grossmann, A., Tchamitchian, P., 1998. Wavelet analysis of signal with gaps. *Journal of Mathematical Physics*
486 39 (8), 4091–4107.
- 487 Graham, G., Watchmaker, F. R. S., 1724. An account of observations made of the variation of the horizontal needle at
488 London, in the latter part of the year 1722, and beginning of 1723. *Philosophical Transactions* 33, 96–107.
- 489 Grossmann, A., Morlet, J., 1984. Decomposition of hardy functions into square integrable wavelets of constant shape.
490 *SIAM Journal on Mathematical Analysis* 15 (4), 723–736.

- 491 Hibberd, F. H., 1985. The geomagnetic sq variation - annual, semi-annual and solar cycle variations and ring current
492 effects. *Journal of Atmospheric and Solar-Terrestrial Physics* 47, 341–352.
- 493 Larsen, J., Cox, C., 1966. Lunar and solar daily variation in the magnetotelluric field beneath the ocean. *Journal of*
494 *Geophysical Research* 71, 4441.
- 495 Le Sager, P., Huang, T. S., 2002. Ionospheric currents and field-aligned currents generated by dynamo action in an
496 asymmetric earth magnetic field. *Journal of Geophysical Research* 107 (A2), 1025.
- 497 Maslova, I., Kokozzka, J., Sojka, L., Zhu, L., 2010. Estimation of sq variation by means of multiresolution and principal
498 component analyses. *Journal of Atmospheric and Solar-Terrestrial Physics* 72, 625–632.
- 499 Matsushita, S., Maeda, H., 1965. On the geomagnetic solar quiet daily variation field during the igy. *Journal of Geophys-*
500 *ical Research* 70 (11), 2535–2558.
- 501 Morlet, J., 1983. Sampling theory and wave propagation. In: Chen, C. (Ed.), *Acoustic Signal/Image Processing and*
502 *Recognition*, in NATO ASI. Springer-Verlag, New York., Vol. 1. pp. 233–261.
- 503 Nesme-Ribes, E., Frick, P., Sokoloff, D., Zakharov, V., Ribes, J. C., Vigouroux, A., Laclare, F., 1995. Wavelet analysis
504 of the maunder minimum as recorded in solar diameter data. *Comptes rendus de l'Académie des sciences. Série II,*
505 *Mécanique, physique, chimie, astronomie* 321 (12), 525–532.
- 506 Oczeretko, E., Swiatecka, J., Kitlas, A., Laudanski, T., Pierzynski, P., 2006. Visualization of synchronization of the
507 uterine contraction signals: running cross-correlation and wavelet running cross-correlation methods. *Medical engi-*
508 *neering & physics* 28 (1), 75–81.
- 509 Parkinson, W. D., 1983. *Introduction to geomagnetism*. Scottish Academy Press, Edinburg and London.
- 510 Price, A. T., 1969. Daily variations of the geomagnetic field. *Space Science Reviews* 9 (2), 151–197.
- 511 Rehman, S., Siddiqi, A. H., 2009. Wavelet based correlation coefficient of time series of saudi meteorological data.
512 *Chaos, Solitons & Fractals* 39 (4), 1764–1789.
- 513 Reiff, P. H., 1983. The use and misuse of statistical analyses. *Solar-Terrestrial Physics: Principles and Theoretical Founda-*
514 *tions*, Proceedings of the Theory Institute held 9-26 August 1982 at Boston College, Chestnut Hill, MA. Edited by
515 R.L. Carolvillano and J.M. Forbes. *Astrophysics and Space Science Library*, Vol. 104. Dordrecht: D. Reidel Publish-
516 ing Co., p.493–522.
- 517 Sastri, J. H., 1988. Equatorial electric fields of ionospheric disturbance dynamo origin. *Annales Geophysicae* 6 (6),
518 635–642.
- 519 Schmucker, U., 1999a. A spherical harmonic analysis of solar daily variations in the years 1964–1965: response esti-
520 mates and source fields for global inductioni. methods. *Issue Geophysical Journal International Geophysical Journal*
521 *International* 136 (2), 439–454.
- 522 Schmucker, U., 1999b. A spherical harmonic analysis of solar daily variations in the years 1964–1965: response estimates
523 and source fields for global inductionii. results. *Geophysical Journal International* 136 (2), 455–476.
- 524 Sizova, L. Z., 2002. The field-aligned currents effect on equatotal geomagnetic field variations. *Advances in Space*
525 *Research* 30, 2247–2252.
- 526 Soon, W., Frick, P., Baliunas, S., 1999. Lifetime of surface features and stellar rotation: a wavelet time-frequency
527 approach. *The Astrophysical Journal* 510 (2), 135–138.
- 528 Stening, R. J., 1971. Longitude and seasonal variations of the sq current system. *Radio Science* 6 (2), 133–137.
- 529 Stewart, B., 1882. *Terrestrial magnetism*. Vol. 16 of *Encyclopaedia Britannica*. Encyclopaedia Britannica Inc., London.
- 530 Takeda, M., 1999. Time variation of global geomagnetic sq field in 1964 and 1980. *Journal of Atmospheric and Solar-*
531 *Terrestrial Physics* 61 (10), 765–774.
- 532 Takeda, M., 2002. The correlation between the variation in ionospheric conductivity and that of the geomagnetic sq field.
533 *Journal of Atmospheric and Solar-Terrestrial Physics* 64 (15), 1617–1621.
- 534 Torrence, C., Compo, G. P., 1998. *A Practical Guide to Wavelet Analysis*. *Bulletin of the American Meteorological*
535 *Society* 79, 61–78.
- 536 Yomoto, K., 2006. The MAGDAS Group, in *Solar Influence on the Heliosphere and Earths Environment: Recent*
537 *Progress and Prospects*. N. Gopalswamy and A. Bhattacharyya, Goa, India.
- 538 Zhao, B., Wan, W., Tschu, K., Igarashi, K., Kikuchi, T., Nozaki, K., Watari, S., Li, G., Paxton, L. J., Liu, L., Ning,
539 B., Liu, J.-Y., Su, S.-Y., Bulanon, H. P., 2008. Ionosphere disturbances observed throughout south- east asia of the
540 superstorm of 20 – 22 november 2003. *Journal of Geophysical Research* 113 (A00A04).

541 **Appendix A.**

542 In order to demonstrate the possibilities of the use of different parameters, and its dependence
543 on the changing characteristics of the chosen wavelet, a sinusoidal signal containing two different
544 frequencies is analyzed by means of the Morlet wavelet in Fig. A.7. This figure contains 3
545 panels. Each panel shows the signal representation and the modulus scalogram using the Morlet

546 wavelet. It is possible to observe that there is a better frequency localization of the Morlet
 547 wavelet transform as the parameter σ increases, see Fig. A.7(a), although it has a worse time
 548 localization. The Fig. A.7(b) occurs the opposite of Fig. A.7(a), it has a better time localization
 549 and worse frequency localization.

550 In Fig. A.7(c), it is also possible to observe that the lower values of the wavelet coefficients
 551 indicate a transition region between different types of movements.

552 We adopted $\omega_0 = 6$ and $\sigma = 1$ that also provides the better possible time-frequency equilib-
 553 rium, see Fig. A.7(b). In this case also, the Morlet wavelet is suited very well for experimental
 554 data analysis because it has a Gaussian envelope. Thus, it allows reaching a reasonable compro-
 555 mise between time and frequency resolutions.

556 Appendix B.

557 In this section, an analysis of a synthetic signal is performed to illustrate the results and
 558 the interpretation of the CWT and the CWT using gapped wavelet techniques, with the purpose
 559 to highlight the differences and the advantages as mentioned earlier. In order to exemplify the
 560 wavelet scalogram expected from this analysis, we defined a synthetic Sq to reproduce the daily
 561 magnetic variation, similarly to the described in Maslova et al. (2010),

$$S_q(t) = \sin\left(\frac{2\pi t}{24}\right) + \sin\left(\frac{4\pi t}{24}\right), \quad (\text{B.1})$$

562 and the noise $R(t)$ as

$$R(t) = 0.5 * V(t) * \sin\left(\frac{2\pi t}{24}\right). \quad (\text{B.2})$$

563 The good Sq estimative $Q(t)$ is given by

$$Q(t) = [S_q(t) + R(t)] * U(t), \quad (\text{B.3})$$

564 where the day to day variability was introduced by the noise variables $V(t)$, $U(t)$ and $R(t)$, where
 565 $V(t)$ was uniformly distributed on $[0, 1]$ and $U(t)$ on $[0.5, 1.5]$.

566 Fig. B.8, from top to bottom, shows the synthetic geomagnetic signal and the wavelet square
 567 modulus (scalogram) with Morlet wavelet. It was possible to identify the two most prevailing
 568 periods (12 and 24-h) due to the quiet variations. Also, we can identify the change of frequencies
 569 introduced by the noise, which indicates that the wavelet analysis is useful for these multi-scale
 570 phenomena.

571 In Fig. B.9, we used the same synthetic signal used in Fig. B.8 but modified with additional
 572 random gaps in the signal. The areas with gaps were signalized by arrows and dashed lines. We
 573 applied the gapped wavelet in this signal. In this new analysis, it was also possible to identify the
 574 quiet geomagnetic variations with periods of 12 and 24-h and there not a significantly difference
 575 in the common intervals of the CWT and gapped scalograms, Figs. B.8 and B.9, respectively.
 576 However, there was a little effect in the boundaries surrounding the gaps regions which led to
 577 some energy lost. This energy lost was not relevant, as seen in the comparison, see Figs. B.8 and
 578 B.9, and can be neglected.

579 In an attempt to fill the gaps, we first tried to use cubic splines interpolation, which led to
 580 an underestimation of high frequencies. As the signals may have many spectral components,
 581 only by using gapped wavelet, the high-frequency part of the spectrum can be reconstructed. For

582 this reason, the gapped wavelet has some advantages over interpolation. However, the gapped
583 wavelet has some limitations, it can only be used if the gap is not larger than the period of
584 analysis.

585 After having applied the CWT and gapped wavelets in the synthetic signal, as presented in
586 Figs. B.8 and B.9, the conclusion was that the gapped wavelet fulfilled better the purposes of this
587 work.

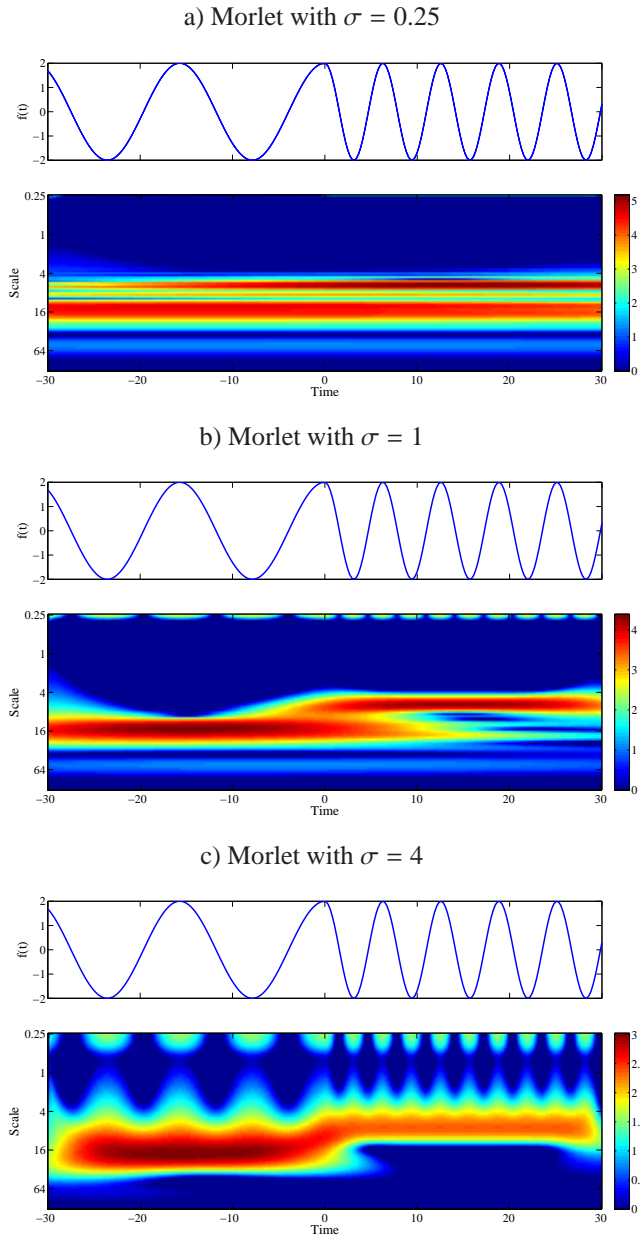


Figure A.7: Representations of an oscillatory function with low and high frequencies spatially displaced and the respective wavelet spectrum for Morlet with different values of parameter σ . The parameter σ assumed the following values of (a) equal to 0.25, (b) 1 and (c) 4.

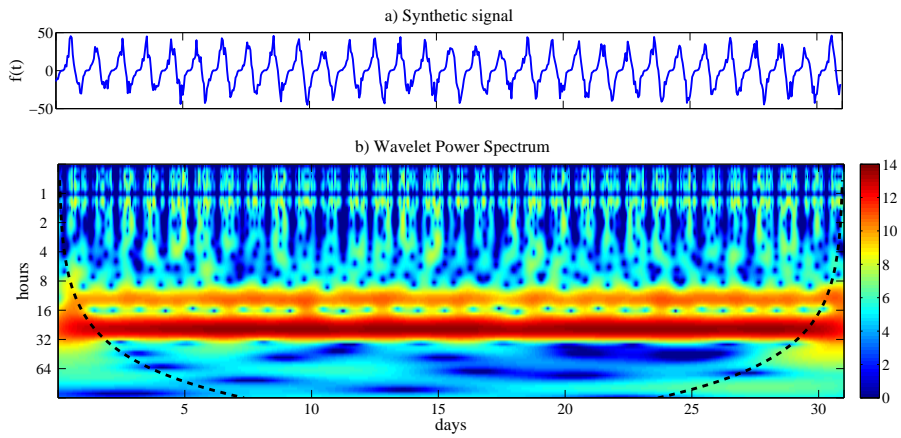


Figure B.8: Spectrograms of synthetic signal consisting of daily magnetic variations. From top to bottom, each panel shows: (a) Synthetic signal and (b) the local wavelet power spectrum using Morlet wavelet, logarithmic scaled representing $\log_2(|W(a, b)|)$.

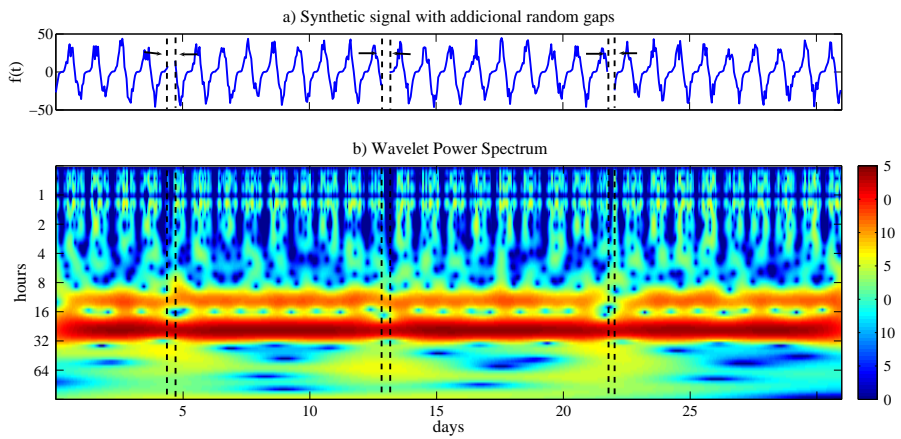


Figure B.9: Spectrograms of synthetic signal with additional random gaps. From top to bottom, each spectrogram shows: (a) Synthetic signal with additional random gaps and (b) the local wavelet power spectrum using gapped wavelet representing $\log_2(|W(a, b)|)$.